Available online at www.sciencedirect.com

ScienceDirect

Procedia Manufacturing 47 (2020) 1490–1495

Procedia MANUFACTURING

www.elsevier.com/locate/procedia

23rd International Conference on Material Forming (ESAFORM 2020)

Mechanical Testing of Metallic Foams for 3d Model and Simulation of Cell Distribution Effects

Edoardo Mancini[a] *, Francesca Campana[b], Daniela Pilone[b] and Marco Sasso[c]

[a]*Università degli studi eCampus, via Isimbardi 10, 22060 Novedrate (CO).*
[b]*Sapienza Università di Roma, DIMA, via Eudossiana 18, 00184 Roma,Italy*
[b]*Sapienza Università di Roma, DICMA, via Eudossiana 18, 00184 Roma,Italy*
[c]*Università Politecnica delle Marche, DIISM, Via Brecce Bianche, 60131 Ancona.*

* Corresponding author. Tel.: +39-071-2204440; *E-mail address:* edoardo.mancini@uniecampus.it

Abstract

Cellular materials have a bulk matrix with a larger number of voids named also cells. Metallic foams made by powder technology represent stochastic closed cells. The related inhomogeneity leads to a scattering of results both in terms of stress–strain curves and maximum strength. Scattering is attributed to relative density variations and local cell discontinuities and it is confirmed also in case of dynamic loading. Finite element simulations through geometrical models that are able to capture the void morphology (named "mesoscale models"), confirm these results and some efforts have been already done to quantify the relationship between shape irregularities and mechanical behavior.
The aim of this paper is to present the dynamic characterization of an AA7075 closed cell material and to calibrate its mesoscale finite element model according to the related cell shape distribution. Specimens have been derived from a small ingot (45x45x100 mm) divided along sections so that morphological analysis and experimental tests have been carried out. Specimens extracted from a half of the ingot have been used for dynamic compression tests by means of a split Hopkinson bar, meanwhile specimens extracted from the other half of the ingot have been dissected for porosity distribution analyses carried out by means of image analysis.
Stress-strain curves obtained from the mechanical tests have been discussed in terms of strain rate and statistical descriptors of the porosity. Successively a 3D-model of the specimen has been generated starting from the Voronoi algorithm, assigning as input the above-mentioned statistical distribution of the porosity. Due to the peculiarity of the cell morphology (e.g. single larger cells), stress-strain localization has been demonstrated as one of the reasons of the scattering found during the experiments. A material model, to reproduce the investigated foam mechanical behavior, has been calibrated. Despite the difference among experiments the material model is able to reproduce all of them. Difference between the model coefficients quantifies roughly the difference due to the local geometry of the cells.

Keywords: Aluminum foams; Image analysis; Impact test; Porosity distribution; Strain rate effect; Voronoi model.

1. Introduction

Aluminum foams have several industrial applications due their unique properties. Among them, the most interesting applications are probably the ones as structural materials in the automotive sector [1]-[4]. Light and stiff parts made of aluminum foams could be useful for reducing the car weight; moreover they can successfully be used as energy absorbers. Efficient energy absorbers should have high absorption capacity, isotropic mechanical properties and a stress-strain curve characterized by a stress plateau after yielding.

Over the years many papers analyzed the behavior of foams under static [5][6] and dynamic loading [7]-[12] highlighting that their characteristics are determined by their heterogeneity deriving from randomly distributed cells. Many different experimental approaches allowed studying the response of

2351-9789
10.1016/j.promfg.2020.04.332

aluminum foams under impact loading. Deformation mode and mechanical behavior of foams having different densities have been deeply investigated [13][14]. The stress plateau stage, which has a dominant role in determining foam energy absorption and damping capability, has been found to be very sensitive to stain rate by several authors, while other authors demonstrated that the effect of strain rate could be ignored [9]. This discrepancy has been investigated and attributed to the interaction between strain rate effect and inertia effect that seems to be predominant under high-speed impact. Strain rate effects depend on the bulk material properties and on the cell distribution and morphology, while the axial-inertia effect depends on the impact speed and determines a large stress on the front surface that produces a front surface densification zone during deformation [9][10].

Considering the complexity of these systems, several approaches have been proposed to model the foam behavior. Some authors [15][16] selected the Voronoi structures to model the geometric configuration of closed cell foams. Other research focused on a mesoscopic model, based on X-ray computed tomography images [7], that employs ellipsoids to model the pores and that introduces their randomness by using selected algorithms. The volume deformation can be also achieved by using experimental techniques as the Digital Volume Correlation (DVC) [17], which exploits the random internal pattern of materials like foams, biological tissues (e.g. bones tissues) or composites. Moreover, in [18] has been proposed an interpolation method based on Bézier curves to reconstruct the volume deformation of homogeneous materials exploiting surface full-field measurements.

A further approach available in literature generated a 3D mesoscopic model that considers heterogeneity and randomness of cell size and thickness of cell walls [11]. These mesoscopic models are used for finite element analyses of metallic foams that allow investigating the effect of impact velocity, material strength and porosity distribution on energy absorption capability of foams.

Aim of this work is to present the dynamic characterization of an AA7075 closed cell foam and to calibrate its mesoscale finite element model according to the related cell shape distribution. Stress-strain curves obtained from the mechanical tests have been discussed in terms of strain rate and statistical descriptors of the porosity. Finally, a material model, to reproduce the investigated foam mechanical behavior, has been calibrated.

2. Materials and method

The analysis investigates AA7075 foam specimens derived from a small ingot (45x45x100) manufactured by compact powder technology. The foam ingot has been divided along sections (Fig. 1) so that morphological analysis and experimental tests have been carried out in similar positions.

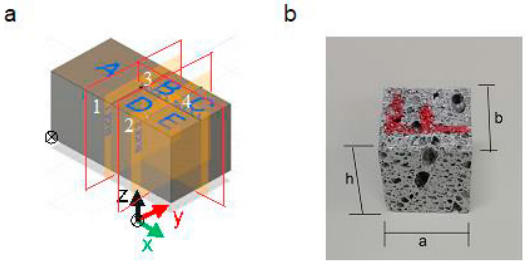

Fig. 1. Sketch showing how the ingot has been sectioned, slice 1 to 4 (a) and an example of specimen derived from A (b).

Specimens extracted from ingot's part A have been used for static and dynamic compression tests, the latter by means of a split Hopkinson bar (Fig. 6), meanwhile specimens extracted from B-C-D-E regions have been dissected for porosity distribution analyses.

Foam ingot was cut minimizing cell wall damage. The surfaces were painted using a black dye with the aim of obtaining a good contrast, essential for image analysis. The specimens were ground with a series of SiC papers and afterwards polished with 1 μm alumina. Image analysis was carried out using Leica Application Suite software: cell size, roundness and mean area were determined. Cell roundness, R is an adimensional value defined by:

$$R = \frac{L^2}{4\pi \cdot A_i \cdot 1.064} \quad (1)$$

where L is the cell perimeter, 1.064 is a factor that takes into account the error introduced in the area calculation by the digitalization of the image, during which continuous perimeters are approximated by discrete rectangles, and A_i is the cell area. R is equal to 1 when the shape is circular, while voids that differ from circles are characterized by R-values greater than 1.

Micro-hardness tests have been carried out on the foam cell walls in order to determine the temper state of the material and select the mechanical property values of the alloy that should be used for simulation. Table 1 shows the mechanical property values selected on the ground of the measured hardness. These values have been used to simulate the foam behavior.

Table 1. Vickers micro-hardness measured on cell walls and alloy mechanical properties used for simulation.

	Mechanical property values
UTS	505 [MPa]
Yield stress	435 [MPa]
Elongation	13%
E	72 [GPa]
HV	160

From these results, the FEA modeling of the specimens has been derived using a Matlab script that implements a random distribution of seeds able to divide the overall volume of the A's specimens in a Voronoi Diagram of the void cells [19]. The

overall number of seeds is defined as a function of the foam Void Volume Fraction (*VVF*) defined as:

$$V_{sphere} = \frac{4}{3} \cdot \pi \cdot r^3 \quad (2)$$

$$num\_seed = floor\left(VVF \cdot \frac{V}{V_{sphere}} \right) \quad (3)$$

where r is the cell mean radius derived from porosity distribution analyses, V is the specimen volume, and *floor* represents the rounding operation to the next lowest integer value. From the Voronoi Diagram an "stl" convex tessellation of the cells is obtained imposing a pseudo-roundness of the cells 2 times greater than that shown by the experimental statistics. This is done, to compensate the smoothing effect introduced by the next mesh size optimization. It converts the "stl" convex tessellation into a regular triangular mesh that can be used for the final tetramesh of the specimen FEA model. In fact, after the mesh size optimization, cell surface tessellation is included in a box that is equivalent to the external surface of the specimen so that a FEA volume mesh is obtained (Fig. 2).

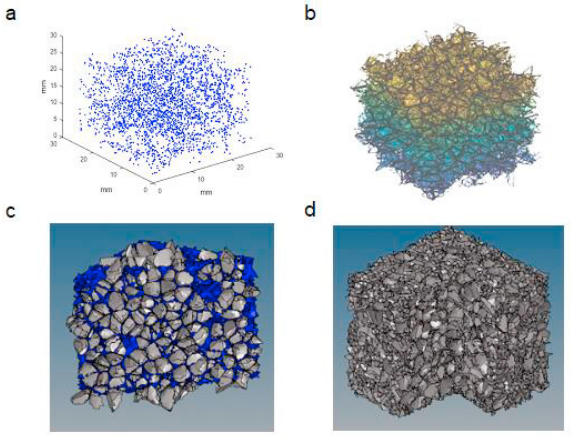

Fig. 2. FEA modeling steps. (a) cell seed; (b) cell convex tessellation; (c) volume definition; (d) FEA solid model.

Simulations have been done through Optistruct/Radioss available in Hyperworks. Material law has been modeled as a Johnson-Cook viscoplastic law according to [20][21], taking into account micro-hardness results. Auto-contact has been provided imposing nodes of the cells as slaves.

3. Experimental Results

3.1. Morphological Analysis

Morphological analysis includes the acquisition of the raw image that is improved with 'pre-processing' techniques, i.e. enhancement and filtering. Enhanced images (Fig. 3 a-d) are then processed to determine cell size (Fig. 3 e-h) and roundness (Fig. 3 i-l)

By observing Fig. 3 it can be highlighted that some big and irregular cavities are present in different sections of the ingot. Although their number is small, their presence could affect the local mechanical response of the material during mechanical tests. In order to analyze the relationship between cell distribution and the material mechanical behavior it is important to study how cells having different size and morphology are distributed in correspondence of each section and, with a complete analysis, how they are distributed inside the all ingot.

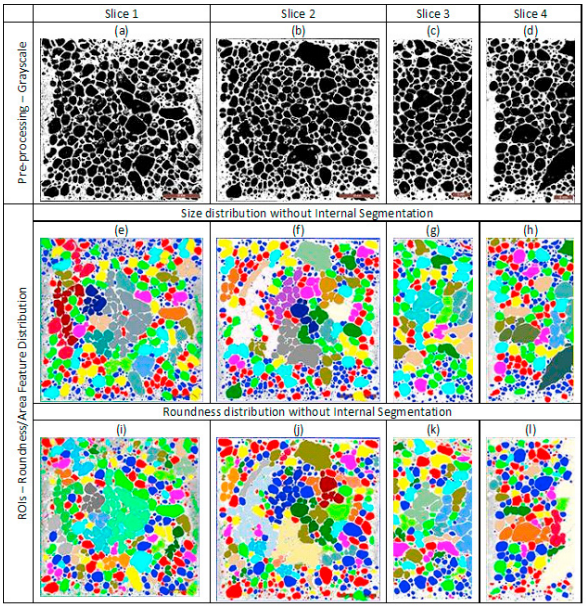

Fig. 3. Image of different sections with regions of interest (ROIs).

The results in Fig. 4 shows that about 80 % of total cells is constituted by cells having an area in the range 0.001 – 1.9 mm^2 and that there is the same size distribution in all the slices. Nevertheless, few cells having large size are present in all the analyzed sections due to random cell agglomeration during foam production.

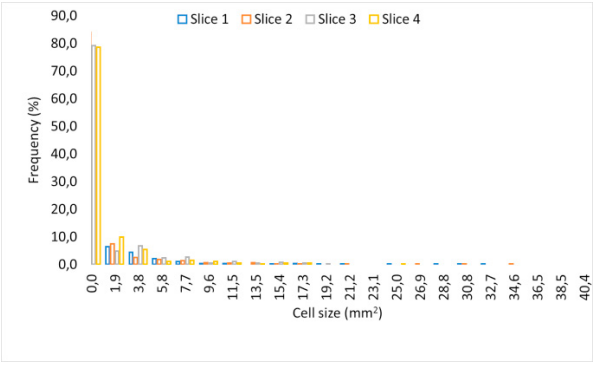

Fig. 4. Cell size distribution in the analyzed sections.

Data reported in Fig. 5 show that more than 70% of cells have a roundness in the range 1-1.36. The analysis results

showed also that slices 1 and 2 show slightly more elongated cells: this can be due to the orientation of the mold during the foaming process.

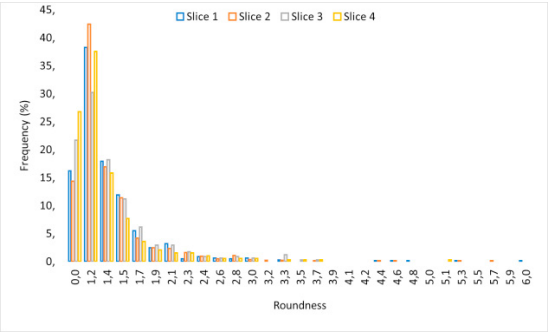

Fig. 5. Roundness distribution in the analysed sections.

The analyzed foam that has an effective density of 0.84 g/cm^3 shows a mean void density of 57.04%. The highest void density has been measured on slices 1 and 2, indicating that the void density increases moving toward the ingot centre part. Data coming from image analysis have been used in the modelling stage.

3.2. Experimental testing

Quasi-static behavior under compression has been investigated in the past by the authors [22] revealing excellent efficiency. Adopting specimens derived from ingots like that of Fig. 1 (with nominal density 0.7 g/cm^3), after removing the external compact surfaces, a constant load was obtained of about 10 kN up to a displacement of 0.055 m (specimens height: 100 mm).

Dynamic tests have been carried out by a direct Split Hopkinson bar [23][24]. All tests have been acquired by a FastCam (Photron® SA4) at 100 kfps. The system set up is reported in Fig. 6.

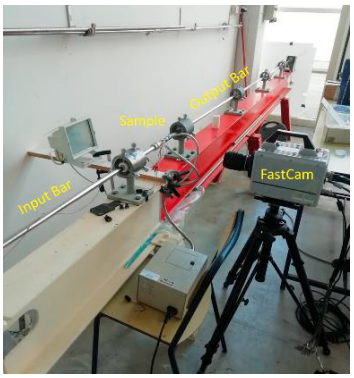

Fig. 6. SHBar set up.

The results, presented in term of engineering stress – strain curves, for samples tested in dynamic conditions, are shown in Fig. 7b. The results highlight a strong dispersion making the foam strain rate sensitive analysis not easily evaluable by the simple curves studies.

However, also the dynamic tests confirm the excellent efficiency shown in the quasi-static (QS) ones. In fact, the curves are characterized by a stiff region with a local peak stress followed by a plateau.

In Fig. 7a is also reported the sample before the test.

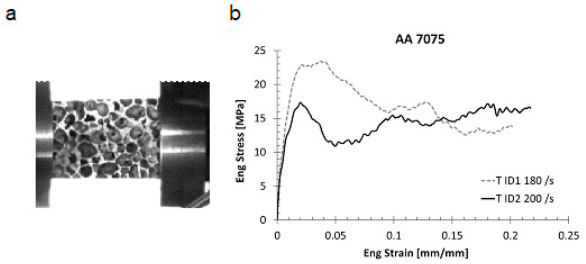

Fig. 7. Direct tension–compression Hopkinson bar (a) specimen and (b) results.

4. 3D Modeling and Simulation

Simulations of the detailed model of the cells have been carried out to assess the role of the cell shape and distribution in the stress-strain curves.

Starting from the morphological analysis, two FEA models have been defined. The first one (named 'P0') represents a random cell distribution obtained with the mean statistical values found in Section 3.1. The second one (named 'P1'). differs from P0 due to a larger cavity provided to mimic a localized outlier cell, like the largest ones found in slice 1, 2 and 4.

Fig. 8. shows one of the significant sections where macroscopic differences among P0 and P1 are visible, in particular nearby the center of the section. Other cavities in the sections have been maintained equal.

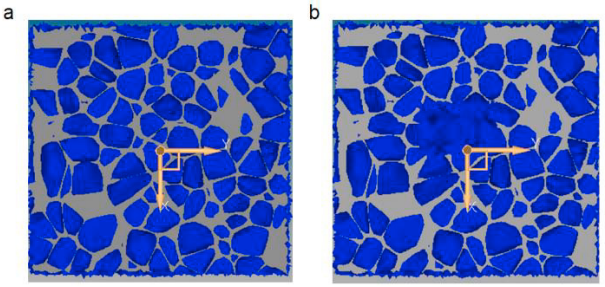

Fig. 8. FEA model P0 (a) and P1 (b). Sections are taken in the middle of the specimens along the direction of the load.

Fig. 9 shows results in both models at the beginning of yielding. It is possible to see a different distribution of stress and strain. P1 induces a localization nearby the large cavity that affects the history of deformation along the specimen.

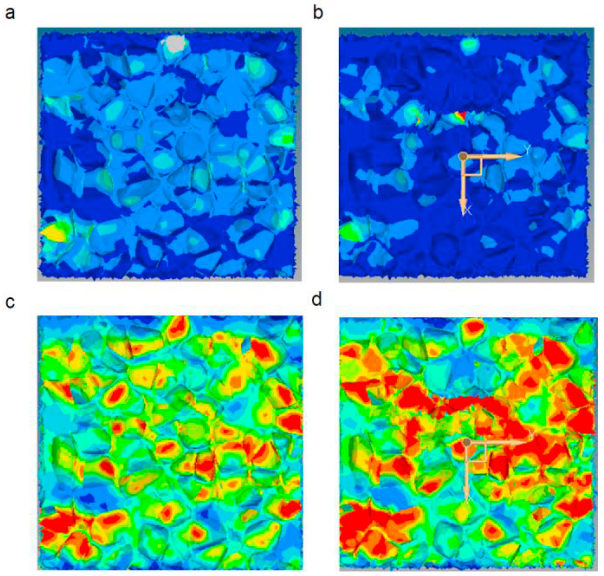

Fig. 9. FEM results. (a) P0 equivalent strain @yielding; (b) P1 equivalent strain @yielding; (c) P0 Von Mises stress (max 410 MPa); (d) P1 Von Mises stress (max 410 MPa).

5. Material model calibration

The results of the experimental activity are implemented within an inverse procedure for material models calibration. The constitutive model proposed by Avalle [25] has been simply modified in order to account for the strain rate sensitivity of the material. The Avalle model has been adopted since it is able to reproduce the first stiff region, with the possible local peak stress, followed by a plateau and, finally, the densification region; from its original formulation, the material strength is multiplied by a dynamic increase factor DIF, which obeys the well-known Johnson-Cook law; the model formulation becomes:

$$\sigma = \left\{ A\left[1 - e^{-(E/A)\varepsilon(1-\varepsilon)^m}\right] + B\left[\varepsilon/(1-\varepsilon)\right]^n \right\} \cdot DIF \qquad (4)$$

where the DIF has the following form:

$$DIF = \left(1 + C \log \frac{\dot{\varepsilon}}{\dot{\varepsilon}_0}\right) \qquad (5)$$

The parameters of best fit for two distinct tests are shown in Table 2. The coefficients of the DIF are borrowed from [20]. How it was expected from the analysis of compression tests, the dispersion results effect is not negligible, and it is noticeable from values reported in Table 2.

Table 2. Material model calibration parameters.

	A	B	E	m	n	C	$\dot{\varepsilon}_0$
T ID1	49.7	26.1	1679	69.9	0.3163	0.058	144
T ID2	53.1	19.2	1516	33.1	0.2297		

Calibration results in terms of engineering stress-strain curves are shown in Fig. 10, where the experimental points are presented in black and the analytical curves are in green. It is clear that the scatter in the experimental results determine the relevant scatter in the model coefficients; The terms A and E do not differ a lot between each other in the two calibrations, whereas the terms B, m and n, which are responsible of the shape of the curve, are seen to vary in a wider range.

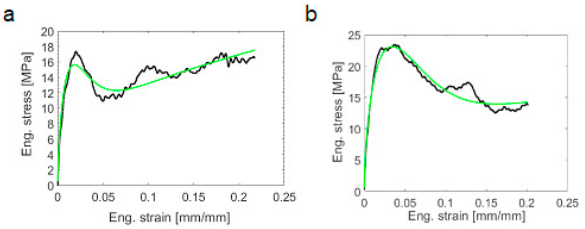

Fig. 10. Calibration of dynamic results of (a) T ID1; (b) T ID2.

6. Discussion

Experimental tests highlight the effect of cell distributions on stress-strain curve scattering. Generally speaking, dispersion is not only related to local instabilities of the activation of the plastic hinges, but it is also related to the macroscopic local deformation and fracture of cell walls when macro-discontinuities are present in the foam structure. It becomes more relevant in dynamic tests and some evidences have been presented here. Dynamic tests reveal different behaviors after the first prominent peak, due to a different history of the deformation gradient. The material model calibration presented in Section 5 quantifies this phenomenon, that has been partially replicated through transient FEA on the 3D mesoscale models P0 and P1. In particular, model P1 shows a clear localized deformation that produces, after the first peak, a steep decrease of the stress-strain curve. In this case, P1 differs from P0 due to the presence of some local large cavities, specifically provided. This makes it similar to specimen ID2.

Fig. 7 shows images of the experimental tests results, confirming the effect of macro-cavities on the global deformation and strength of the specimens.

7. Conclusion

Parts made of aluminum foams could be useful for reducing weight, moreover they can by successfully used as energy absorbers. The capacity to absorb energy is related mainly to the stress plateau stage that could be sensible or not to strain rate.

Dynamic tests by a direct Split Hopkinson bar have been carried out. They highlighted a considerable result dispersion that makes difficult to interpret the results. Although the bulk material is sensitive to strain rate the considerable dispersion of the results made the foam strain rate sensitivity analysis not evaluable by the simple curves study.

From the morphological analysis it is evident that few cells having large size are present in all the analyzed sections, so they could be significant for the strong dispersion of the dynamic

results. Implementing a more accurate procedure, that through the mesoscale modeling could allow to evaluate the strain rate effect with some uncertainty, is of fundamental importance.

A mesoscale FEA model, that is able to reproduce the cells according to a statistical distribution derived from the morphological analysis of the cells, has been implemented and tested with and without the presence a large size cells. In the model, the strain rate effect has been taken into account by Johnson-Cook law. The simulation confirmed the strong influence of the irregular cavities on the results dispersion.

An analytical model has been calibrated by an inverse procedure in order to reproduce the behavior of tested foam. The scatter in the experimental results determined the relevant scatter in the model coefficients too. It confirms the necessity of a model able to take into account cell distribution effect, in fact a more accurate stress-strain evaluation is request when cell size is relevant compared to the specimen length.

As a future work, the present study together with the sample topography will be useful to implement a procedure for the definition of a material equivalent able to reproduce, with a specific scatter, the foam behavior in QS and dynamic conditions.

References

[1] Ashby MF, Evans AG, Fleck NA, Gibson LJ, Hutchinson JW, Wadley HNG. Metal Foams, Oxford: Butterworth-Heinemann; 2000.

[2] Banhart J. Manufacture, characterisation and application of cellular metals and metal foams. Prog Mater Sci 2001;46:559-632.

[3] Zhao B, Gain AK, Ding W, Zhang L, Li X, Fu Y. A review on metallic porous materials: pore formation, mechanical properties, and their applications. Int J Adv Manuf Technol 2018;95:2641-2659.

[4] Nazir A, Abate KM, Kumar A, Jeng J-Y. A state-of-the-art review on types, design, optimization, and additive manufacturing of cellular structures. Int J Adv Manuf Technol 2019;104:3489-3510.

[5] Campana F, Cortese L, Pilone D. Property variations in large AlSi7 alloy foam ingots. Mat Sci Eng A-Struct 2012; 556: 400-407.

[6] Liang X, Luo H, Mu Y, Chen M, Ye J, Chi D. Quasi-static and Dynamic Compression of Aluminum Foam at Different Temperatures. J Mater Eng Perform 2019;28:4952-4963.

[7] Liu X, Zhang J, Fang Q, Wu H, Zhang Y. Response of closed-cell aluminum foams under static and impact loading: Experimental and mesoscopic numerical analysis. Int J Imp Eng 2017;110:382-394.

[8] Pang X, Du H. Dynamic characteristics of aluminium foams under impact crushing. Composites Part B: Engineering 2017;112:265-277.

[9] Wang P, Xu S, Li Z, Yang J, Zhang C, Zheng H, Hu S. Experimental investigation on the strain-rate effect and inertia effect of closed-cell aluminum foam subjected to dynamic loading. Mat Sci Eng A-Struct 2015;620:253-261.

[10] Liu YD, Yu JL, Zheng ZJ, Li JR. A numerical study on the rate sensitivity of cellular metals. Int. J. Solids Struct 2009;46:3988-3998.

[11] Fang Q, Zhang J, Zhang Y, Liu J, Gong Z. Mesoscopic investigation of closed-cell aluminum foams on energy absorption capability under impact. Compos Struct 2015;124:409-420.

[12] Liu J, He S, Zhao H, Li G, Wang M. Experimental investigation on the dynamic behaviour of metal foam: From yield to densification, Int J Imp Eng 2018;114:69-77.

[13] Campana F, Mancini E, Pilone D, Sasso M. Strain rate and density-dependent strength of AlSi7 alloy foams. Mat Sci Eng A-Struct 2016;651:657-667.

[14] Liu H, Cao ZK, Luo HJ, Shi JC, Yao GC. Performance of closed-cell aluminum foams subjected to impact loading. Mat Sci Eng A-Struct 2013;570:27-31.

[15] Zhang CY, Tang LQ, Yang B, Zhang L, Huang, XQ, Fang DN. Meso-mechanical study of collapse and fracture behaviors of closed-cell metallic foams. Comp Mater Sci 2013;79:45-51.

[16] Zheng Z, Wang C, YuJ, Reid SR, Harrigan JJ. Dynamic stress-strain states for metal foams using a 3D cellular model. J Mech Phys Solids 2014;72:93-114.

[17] Bay BK, Smith TS, Fyhrie DP, Saad M. Digital volume correlation: Three-dimensional strain mapping using X-ray tomography. Exp Mech 1999;39:217–226.

[18] Rossi M, Cortese L, Genovese K, Lattanzi A, Nalli F, Pierron F. Evaluation of Volume Deformation from Surface DIC Measurement. Exp Mech 2018;58:1181–1194.

[19] Bici M, Campana F, De Michelis M. Mesoscale Modeling of Cellular Materials for Finite Element Analysis. Comput-Aided Des Applic 2017;14:760-769.

[20] Sasso M, Forcellese F, Simoncini M, Amodio D, Mancini E. High Strain Rate Behaviour of AA7075 Aluminum Alloy at Different Initial Temper States. Key Eng. Mater 2015;651-653:114-119.

[21] Johnson R, Cook WH. A constitutive model and data for metals subjected to large strains, high strain rates and high temperatures. Int Symp Ballistics the Hague Netherlands 1983;7:541-547.

[22] Campana F, Pilone D. Effect of wall microstructure and morphometric parameters on the crush behaviour of Al alloy foams. Mater Sci Eng A 2008;479:58-64.

[23] Mancini E, Sasso M, Rossi M, Chiappini G, Newaz G, Amodio D. Design of an Innovative System for Wave Generation in Direct Tension–Compression Split Hopkinson Bar. J Dyn Behav Mater 2015;1:201–213.

[24] Sasso M, Antonelli M G, Mancini E, Radoni M, Amodio D. Experimental and numerical characterization of a polymeric Hopkinson bar by DTMA. Int J Impact Eng 2017; 103: 50-63.

[25] Avalle M, Belingardi G, Ibba A. Mechanical models of cellular solids: Parameters identification from experimental tests. Int J Impact Eng 2007;34:3-27.